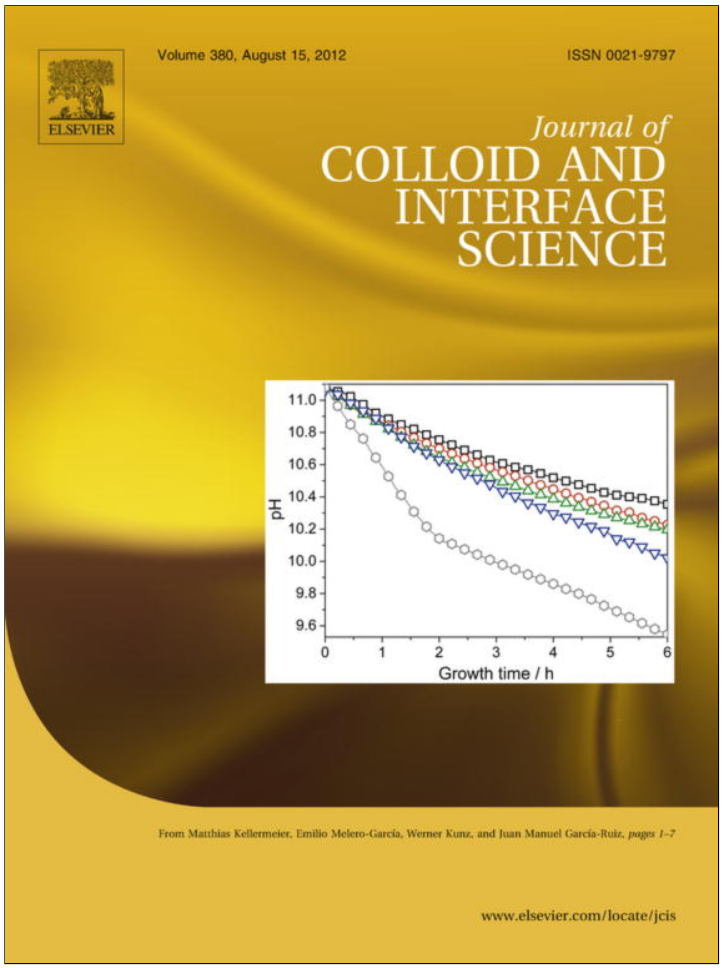

Journal of Colloid and Interface Science 380 (2012) 213–221

Contents lists available at SciVerse ScienceDirect

Journal of Colloid and Interface Science

www.elsevier.com/locate/jcis

Equilibrium properties of charged spherical colloidal particles suspended in aqueous electrolytes: Finite ion size and effective ion permittivity effects

José Juan López-García [a], José Horno [a,*], Constantino Grosse [b,c]

[a] Departamento de Física, Universidad de Jaén, Campus Las Lagunillas, Ed. A-3, 23071 Jaén, Spain
[b] Departamento de Física, Universidad Nacional de Tucumán, Av. Independencia 1800, 4000 San Miguel de Tucumán, Argentina
[c] Consejo Nacional de Investigaciones Científicas y Técnicas, Av. Rivadavia 1917, 1033 Buenos Aires, Argentina

ARTICLE INFO

Article history:
Received 6 March 2012
Accepted 8 May 2012
Available online 16 May 2012

Keywords:
Ion size effect
Ion permittivity effect
Modified Poisson–Boltzman equation
Electrical double layer

ABSTRACT

The equilibrium properties of a charged spherical colloidal particle immersed in an aqueous electrolyte solution are examined using an extension of the Standard Electrokinetic Model that takes into account the finite ion size by modeling the aqueous electrolyte solution as a suspension of polarizable insulating spheres in water. We find that this model greatly amplifies the steric effects predicted by the usual modified Poisson–Boltzmann equation, which only imposes a restriction on the ability of ions to approach one another. This suggests that a solution of the presented model under nonequilibrium conditions could have important consequences in the interpretation of dielectric and electrokinetic data in colloidal suspensions.

1. Introduction

When solid objects (colloidal particles, interfaces, membranes, proteins, etc.) are placed in contact with an aqueous electrolyte solution, they usually acquire a surface charge and spatial distributions of charge and electric potential, known as the electrical double layer, appear close to the interface. This structure plays a crucial role in colloid and polymer science, biophysics, medicine, and numerous separation technologies (e.g., water and wastewater filtration, membrane filtration, protein and cell separation, immobilization of enzymes, etc.) [1–3]. This is the reason for the great importance and interest in theoretical models of the electrical double layer structure. The theoretical model based on the Poisson–Boltzmann (PB) equation is an acknowledged and widely used description of the diffuse part of the equilibrium electric double layer [4–10]. However, it is not difficult to point at a number of imperfections in the Poisson–Boltzmann theory, such as the finite size of the ions is neglected, particle–ion interactions are not taken into account, the permittivity of the medium is assumed to be constant, and incomplete dissociation of the electrolyte is ignored [11].

In the last two decades, various attempts have been made to modify the classic PB equation so that the ionic interactions can be accounted for [12–18]. All these works are based on the assumption that the ion density cannot surpass anywhere a finite value c_i^{max} (in mol/m^3), where the lower index i corresponds to the ion type. This led to the following main consequence: the ion density close to a charged interface cannot attain unrealistically high values, improving on the results predicted by PB equation. Comparison with theories based on Monte Carlo simulations shows that this modification of the Poisson–Boltzmann (MPB) equation works very well for a wide range of situations [19]. However, it still presents one important shortcoming: the correction of the MPB over the PB equation only appears at high surface charges and for high bulk electrolyte concentrations [17,20]. In the last years, the theoretical model based on the MPB equation has been extended incorporating a distance of closest approach of ions to the particle surface obtaining, as main consequence, that the excluded volume effect is not negligible even for weakly charged particles suspended in low concentration electrolyte solutions [21–23]. However, in order to fit experimental data, it is necessary to consider effective ionic radii much larger than the hydrated ionic radii, which is physically objectionable [24,25].

In any case, it is interesting to point out that the theories presented in these studies do not imply that ions have a finite size: there is only a restriction on their ability to approach one another or the surface of the particle. On the contrary, a finite ion size implies that ions have a finite volume that can no longer be occupied by the suspending medium. In a recent letter [26], we presented an extension of the MPB equation considering that ions can be modeled as insulating spheres with a permittivity different from that of the surrounding medium. We showed that this led to the following main consequences:

* Corresponding author. Fax: +34 953 212838.
E-mail address: jhorno@ujaen.es (J. Horno).

0021-9797/$ - see front matter © 2012 Elsevier Inc. All rights reserved.
http://dx.doi.org/10.1016/j.jcis.2012.05.012

(1) The presence of ions in the suspending medium should modify its permittivity. Moreover, since the ion concentration near a charged interface strongly depends on the distance to its surface, the electrolyte solution permittivity should also depend on this distance.
(2) A variable permittivity of the electrolyte solution leads to the appearance of a new force term acting on an ion since charges tend to move into regions of higher permittivity (a consequence of the so-called Born energy).
(3) The dielectric sphere representing an ion gets polarized by the local electric field and acquires a dipole moment. Therefore, an additional dielectrophoretic force acting on the dipole will appear wherever the local field is nonuniform.
(4) The steric effects predicted by the usual MPB equation are greatly amplified, even for reasonable effective ionic radii.

In the present work, we apply this formalism, originally written for plane geometry, for the description of the equilibrium properties of colloidal suspensions. In doing so, we include the requirement that ions cannot come closer to the particle surface than a minimum approach distance, an effect we omitted for simplicity in the above-mentioned letter. We discuss in more detail the individual contributions of the different effects and determine their dependences on the ion size and effective ion permittivity.

2. Theory

Let us consider a spherical colloidal particle of radius a and surface charge density σ_S immersed in an infinite solution made of m ionic species represented by insulating spheres with effective radius R_i, permittivity ε_i, signed valence z_i, and bulk concentration (in mol/m^3) c_i^∞ (with $i \in \{1, 2, \ldots, m\}$) suspended in a continuous medium with permittivity ε_w.

2.1. Permittivity of the solution

The permittivity ε_e of the solution can be determined using the Maxwell mixture formula [27], which is quite accurate over the whole concentration range when the dispersions have a lower permittivity than the suspending medium:

$$\frac{\varepsilon_e - \varepsilon_w}{\varepsilon_e + 2\varepsilon_w} = \sum_{i=1}^{m} \phi_i \frac{\varepsilon_i - \varepsilon_w}{\varepsilon_i + 2\varepsilon_w} \tag{1}$$

In this expression, ϕ_i is the local value of the volume fraction occupied by ions of species i:

$$\phi_i = N_A c_i \frac{4\pi}{3} R_i^3 \tag{2}$$

where N_A is the Avogadro number and c_i is the local concentration (in mol/m^3) of ionic species i.

The effective ionic radius is related to the maximum value of the ion density by means of:

$$c_i^{\max} = \frac{p}{\frac{4\pi}{3} R_i^3 N_A} \tag{3}$$

where p is the packing coefficient ($p = 1$ for perfect packing, $p = \pi/3\sqrt{2} \approx 0.74$ for close packing, $p \approx 0.64$ for random close packing, $p = \pi/6 \approx 0.52$ for simple cubic packing).

Therefore, Eq. (1) can be finally written as:

$$\varepsilon_e = \varepsilon_w \frac{1 + 2p\sum_{i=1}^{m} \frac{c_i}{c_i^{\max}} \frac{\varepsilon_i - \varepsilon_w}{\varepsilon_i + 2\varepsilon_w}}{1 - p\sum_{i=1}^{m} \frac{c_i}{c_i^{\max}} \frac{\varepsilon_i - \varepsilon_w}{\varepsilon_i + 2\varepsilon_w}} \tag{4}$$

This expression is more general than the linear dependence of the electrolyte solution permittivity on the ion concentrations used in previous works. For example, the expression used in a recent contribution, Ref. [28], is simply the first order linear expansion of Eq. (4), so that it should only be valid for low ion concentrations and should greatly overestimate the permittivity decrement in regions of extremely high ion concentration close to the charged interface.

2.2. Poisson equation

To determine the electric potential distribution, the Poisson equation, relating the electric potential, Ψ, to the volume charge density, ρ, written taking into account the spatial dependence of the electrolyte solution permittivity, will be used.

$$\nabla \cdot (\varepsilon_e \vec{E}) = \varepsilon_e \nabla \cdot \vec{E} + \vec{E} \cdot \nabla \varepsilon_e = -\varepsilon_e \nabla^2 \Psi - \nabla \Psi \cdot \nabla \varepsilon_e = \rho = eN_A \sum_{i=1}^{m} z_i c_i \tag{5}$$

where e is the elementary charge and $\vec{E}$ is the electric field.

Taking into account the radial symmetry of the problem, Eq. (5) can be rewritten as:

$$\frac{1}{r^2} \frac{d}{dr}\left(r^2 \frac{d\Psi}{dr}\right) = -\frac{eN_A}{\varepsilon_e} \sum_{i=1}^{m} z_i c_i - \frac{d \ln \varepsilon_e}{dr} \frac{d\Psi}{dr} \tag{6}$$

2.3. Ionic concentrations

Due to their finite size, ions of species i cannot come closer to the particle surface than to an effective distance of minimum approach that, for simplicity, will be considered equal to the corresponding effective ionic radius, R_i. The simplest way to include this effect in the theoretical model is to consider that for the region $a < r < a + R_i$ the concentration of the ionic species i vanishes.

On the other hand, the distribution of ionic concentration inside the solution will be given by the competition among the following macroscopic average forces (per mol) acting upon the ions:

(i) The electric force:

$$\vec{F}_i^E = z_i e \vec{E} = -z_i e \nabla \Psi \tag{7}$$

(ii) The thermal force due to the random ion movement:

$$\vec{F}_i^T = -kT \nabla \ln(c_i) \tag{8}$$

where k is the Boltzmann constant and T is the absolute temperature of the system.

(iii) The viscous drag force that appears wherever the ion velocity is different from the local fluid velocity:

$$\vec{F}_i^V = -\frac{\vec{v}_i - \vec{v}}{\lambda_i} \tag{9}$$

where $\vec{v}_i$ is the velocity of ions of species i, λ_i is their mobility, and $\vec{v}$ is the fluid velocity.

(iv) The steric force limiting the ability of ions to approach one another that appears when ion size effects are taken into account:

$$\vec{F}_i^S = -kT \nabla \ln \gamma_i \tag{10}$$

where γ_i is the activity coefficient of the ionic species i. As in our previous works, we use for simplicity a Bikerman [30] type expression for the activity coefficients:

$$\gamma = \gamma_i = \frac{1}{1 - \sum_{i=1}^{m} \frac{c_i}{c_i^{\max}}} \tag{11}$$

(v) The Born force that appears when the permittivity of the solution is allowed to change [29]. The electrostatic energy of an ion can be obtained integrating the energy density corresponding to its electric field, E:

$$W = \frac{\varepsilon_e}{2}\int_{R_i}^{\infty} E^2 dV = \frac{\varepsilon_e}{2}\int_{R_i}^{\infty}\left(\frac{z_i e}{4\pi\varepsilon_e r^2}\right)^2 4\pi r^2 dr = \frac{z_i^2 e^2}{8\pi\varepsilon_e R_i} \tag{12}$$

This energy depends on the permittivity of the surrounding medium so that, wherever this permittivity changes, ions will tend to move to regions of higher permittivity in order to lower their energy. The corresponding force acting on both counterions and co-ions is:

$$\vec{F}_i^B = -\nabla W = -\nabla\frac{z_i^2 e^2}{8\pi\varepsilon_e R_i} = -\frac{z_i^2 e^2}{8\pi R_i}\nabla\left(\frac{1}{\varepsilon_e}\right) \tag{13}$$

(vi) The dielectrophoretic force that appears when ions are assumed to behave as dielectric spheres. Under the action of an external field, hydrated ions should then become polarized by an external field acquiring an induced dipole moment:

$$\vec{m}_i = 4\pi\varepsilon_e R_i^3\frac{\varepsilon_i-\varepsilon_e}{\varepsilon_i+2\varepsilon_e}\vec{E} \tag{14}$$

Note that this expression differs from that used in [28], which is similar to Eq. (14) except that the permittivity of water ε_w is substituted for the electrolyte solution permittivity ε_e. This implies that the direct influence of the electrolyte solution permittivity variation on the dielectrophoretic force is neglected in [28].

If the local field is nonuniform, the dielectrophoretic force given by

$$\vec{F}_i^D = (\vec{m}_i\cdot\nabla)\vec{E} = 2\pi\varepsilon_e R_i^3\frac{\varepsilon_i-\varepsilon_e}{\varepsilon_i+2\varepsilon_e}\nabla(E^2) \tag{15}$$

will attract ions toward regions of stronger (weaker) field if their equivalent permittivity is higher (lower) than that of the surrounding medium. Generally, the ion permittivity is lower than that of the electrolyte solution, so that the dielectrophoretic force tends to diminish the concentration of both counterions and co-ions close to the particle surface.

If inertial effects related to ions are neglected, the total force acting on them must be equal to zero,

$$\vec{F}_i^E + \vec{F}_i^T + \vec{F}_i^V + \vec{F}_i^S + \vec{F}_i^B + \vec{F}_i^D = 0 \tag{16}$$

so that the ionic flows (in mol/(s m^2)) can be written as:

$$c_i\vec{v}_i = -D_i c_i\left\{\nabla\left[\ln(\gamma c_i) + \frac{z_i^2 e^2}{8\pi kTR_i}\frac{1}{\varepsilon_e} + \frac{z_i e}{kT}\Psi\right] - \frac{2\pi R_i^3}{kT}\varepsilon_e\frac{\varepsilon_i-\varepsilon_e}{\varepsilon_i+2\varepsilon_e}\nabla(\vec{E}^2)\right\} + c_i\vec{v} \tag{17}$$

where the Einstein expression relating the mobility with the diffusion coefficient has been used. Note that Eq. (17) reduces to the Nernst–Planck equation if the ionic permittivity is assumed to be equal to that of the medium and ionic size effects are neglected, that is, $\gamma = 1$.

In equilibrium, the fluid and ion velocities vanish so that Eq. (17) simplifies to:

$$\frac{d}{dr}\left[\ln(\gamma c_i) + \frac{z_i^2 e^2}{8\pi kTR_i}\frac{1}{\varepsilon_e} + \frac{z_i e}{kT}\Psi - \frac{2\pi R_i^3}{kT}\int\varepsilon_e\frac{\varepsilon_i-\varepsilon_e}{\varepsilon_i+2\varepsilon_e}\frac{d\vec{E}^2}{dr}dr\right] = 0 \tag{18}$$

where the spherical symmetry in the problem has been taken into account.

The solution of Eq. (18) is:

$$c_i = \frac{K_i}{\gamma}e^{f_i}\exp\left(-\frac{z_i e\Psi}{kT}\right) \tag{19}$$

where

$$f_i = \frac{z_i^2 e^2}{8\pi kTR_i}\left(\frac{1}{\varepsilon_e^\infty}-\frac{1}{\varepsilon_e}\right) - \frac{4\pi eR_i^3}{kT}\int_r^\infty\frac{\varepsilon_e(\varepsilon_i-\varepsilon_e)}{\varepsilon_i+2\varepsilon_e}\frac{d\Psi}{dr}\frac{d^2\Psi}{dr^2}dr \tag{20}$$

and K_i is an integration constant.

2.4. Boundary conditions

To complete the theoretical model, it is necessary to specify appropriate boundary conditions:

$$\left.\frac{d\Psi(r)}{dr}\right|_a = -\frac{\sigma_s}{\varepsilon_e(a)} \tag{21}$$

$$\Psi(a+R_i)^- = \Psi(a+R_i)^+ \tag{22}$$

$$\varepsilon_e(a+R_i)^-\left.\frac{d\Psi(r)}{dr}\right|_{(a+R_i)^-} = \varepsilon_e(a+R_i)^+\left.\frac{d\Psi(r)}{dr}\right|_{(a+R_i)^+} \tag{23}$$

$$\Psi(r\to\infty)\to 0 \tag{24}$$

$$c_i(r\to\infty)\to c_i^\infty \tag{25}$$

Condition (21) is the Gauss law relating the surface charge density of the particle σ_S to the normal component of the electric field at its surface; Eqs. (22) and (23) express the continuity of the electric potential and of the normal component of the electric displacement at the distance of closest approach of ions to the particle surface; Eq. (24) expresses the choice of the potential origin at $r\to\infty$; and Eq. (25) requires that the ionic concentration attains the bulk concentration as $r\to\infty$.

Using boundary conditions (24) and (25), the integration constants K_i can be determined

$$K_i = \frac{1}{1-\sum_{i=1}^m\frac{c_i^\infty}{c_i^{\max}}}c_i^\infty = \gamma^\infty c_i^\infty \tag{26}$$

2.5. Numerical solution

For computational reasons, it is convenient to use the spatial variable

$$q = \frac{a}{r}\exp[\kappa(a-r)] \tag{27}$$

where

$$\kappa = \sqrt{\frac{e^2N_A\sum_{i=1}^m z_i c_i^\infty}{kT\varepsilon_e^\infty}} \tag{28}$$

is the Debye screening length. This transforms the above presented theoretical model into:

$$\frac{d^2y}{dq^2} + \frac{(\kappa a)^2}{q\left(\frac{a}{r}+\kappa a\right)^2}\frac{dy}{dq} = \begin{cases} -\frac{e^2N_A\frac{\gamma^\infty}{\gamma}\sum_{i=1}^m z_i c_i^\infty e^{f_i}\exp(-z_i y)}{q^2\left(\frac{a}{r}+\kappa a\right)^2 kT\varepsilon_e} - \frac{d\ln\varepsilon_e}{dq}\frac{dy}{dq} & 0\leqslant q\leqslant\frac{a}{a+R}\exp(-\kappa R) \\ 0 & \frac{a}{a+R}\exp(-\kappa R) < q\leqslant 1 \end{cases} \tag{29}$$

where

$$y = \frac{e\Psi}{kT} \tag{30}$$

$$f_i = \frac{z_i^2 e^2}{8\pi kTR_i}\left(\frac{1}{\varepsilon_e^\infty}-\frac{1}{\varepsilon_e}\right) - \frac{4\pi kTR_i^3}{e}\int_q^0\frac{\varepsilon_e(\varepsilon_i-\varepsilon_e)}{\varepsilon_i+2\varepsilon_e} \times\frac{dy}{dq}\left[q^2\left(\frac{1+\kappa r}{r}\right)^2\frac{d^2y}{dq^2} + q\frac{(\kappa r)^2+2\kappa r+2}{r^2}\frac{dy}{dq}\right]dq \tag{31}$$

$$\varepsilon_e = \varepsilon_w \frac{1 + 2p\sum_{i=1}^{m} \phi_i \frac{\varepsilon_i - \varepsilon_w}{\varepsilon_i + 2\varepsilon_w}}{1 - p\sum_{i=1}^{m} \phi_i \frac{\varepsilon_i - \varepsilon_w}{\varepsilon_i + 2\varepsilon_w}} \tag{32}$$

$$\phi_i = \frac{c_i^{\infty}}{c_i^{\max}} \frac{\gamma^{\infty}}{\gamma} e^{f_i} \exp(-z_i y) \tag{33}$$

and it has been considered that all the ionic species have the same effective radius R.

The theoretical model was solved using a finite difference scheme, that is, discretizing the space, for which a change of the spatial variable was made, Eq. (27), in order to obtain a finite region of study. Then, the following algorithm was used:

1. The starting point is the solution of Eq. (29) for an uncharged particle: $\Psi(q) = 0, f_i(q) = 0, c_i(q) = c_i^{\infty}$ and $\varepsilon_e(q) = \varepsilon_e^{\infty}$, where ε_e^{∞} is calculated using Eq. (4).
2. The particle surface charge is slightly increased:
   - 2.1. Eq. (29) is linearized and solved using the previous values for $f_i(q)$, $c_i(q)$, and $\varepsilon_e(q)$.
   - 2.2. Eq. (33) is used to calculate ϕ_i.
   - 2.3. These values are used to calculate new values of $\varepsilon_e(q)$ using Eq. (32).
   - 2.4. These values are used to calculate new values of $f_i(q)$ using Eq. (31).
   - 2.5. Points 2.1–2.4 are repeated until convergence is attained.
3. Point 2 is repeated until the desired particle surface charge is attained.

It must be noted that because the variable y changes rapidly near the surface of the particle ($q = 1$), an appropriate simulation space grid must be modeled. In this work, the q-space grid is automatically adapted to the evolution of the potential profiles. If during the simulation strong changes of y with q are detected in any region of the q coordinate, more grid points are added into this region to ensure good accuracy and moderate CPU times.

3. Results

The calculations were performed considering a spherical colloidal particle bearing a positive surface charge density σ_S and suspended in a binary aqueous electrolyte solution. We use a hydrated ion relative permittivity value of 20 since, according to [31], typical values for univalent and divalent ions are 25 and 8, respectively. The choice of the solvated ionic radius value of 0.3 nm was based on the usual 0.3–0.4 nm range obtained from mobility measurements [24]. The remaining system parameters are given in Table 1.

Fig. 1 shows the counterion density profiles for different model approximations. The black line, included for comparison, represents the classical Poisson–Boltzmann solution determined solely by the electric and thermal forces. The red line represents the modified Poisson–Boltzmann solution that additionally includes the steric forces among ions. The counterion concentration no longer grows to unreasonably high values but rather attains a maximum allowed value $c_1^{\max}$ that is related to the finite ion size,

Table 1
Parameter values used in the simulation except when indicated otherwise.

$e = 1.602 \times 10^{-19}$ C	$N_A = 6.022 \times 10^{23}$ mol^{-1}	$k = 1.381 \times 10^{-23}$ J/K
$T = 298$ K	$a = 100$ nm	$\sigma_S = 0.3$ C/m^2
$\varepsilon_w = 80\varepsilon_0$	$\varepsilon_i = 20\varepsilon_0$	$p = 0.74$
$z_1 = -1$	$c_1^{\infty} = 100$ mol/m^3	$R_1 = 0.3$ nm
$z_2 = 1$	$c_2^{\infty} = 100$ mol/m^3	$R_2 = 0.3$ nm

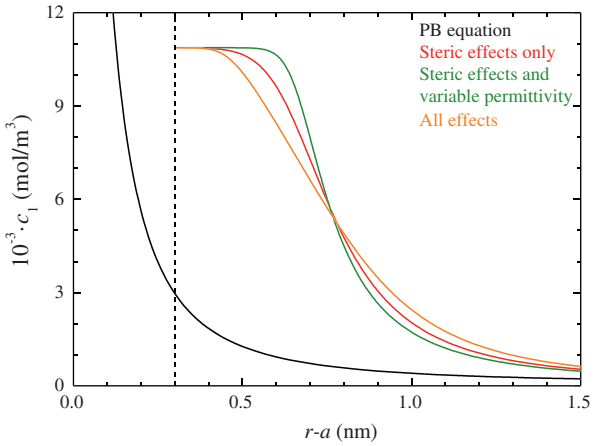

Fig. 1. Counterion density profiles around the suspended particle for the indicated model approximations. Used parameter values given in Table 1.

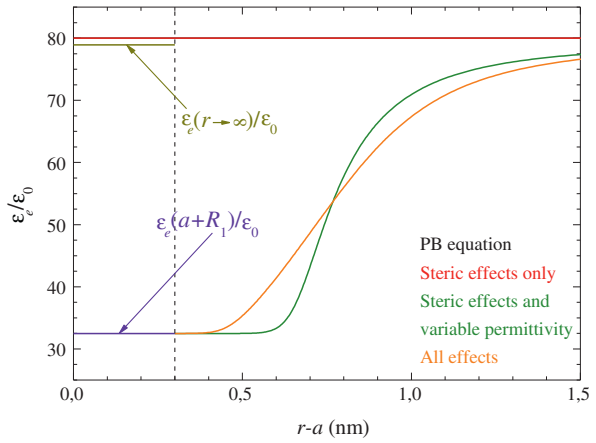

Fig. 2. Electrolyte solution permittivity profiles around the suspended particle for the indicated model approximations. Used parameter values given in Table 1.

Eq. (3). Moreover, this finite size determines a minimum approach distance of ions to the particle surface leading to a vanishing ion concentration at smaller distances. The green line further includes the effect of the variable electrolyte solution permittivity. The high ion concentration close to the particle lowers the permittivity, which increases the radial electric field of the particle. This attracts more counterions to the saturation layer increasing its thickness. However, since the particle surface charge is kept constant, the total surface density of counterions and co-ions must also remain constant, which determines the more abrupt drop of the green line as compared to red one. Finally, the orange line includes all the considered effects: steric, variable permittivity, Born, and dielectrophoresis. The last two terms tend to lower the counterion concentration: the Born force pulls ions to regions of higher permittivity, while the dielectrophoretic force pulls ions to regions of lower electric field gradient because the induced dipole moment of the dielectric sphere representing the ion is negative. As can be seen, the effect of these two forces is stronger than the effect of the variable permittivity in the considered example, so that the saturation layer is thinner for the orange line than for the red one.

Fig. 2 shows the corresponding electrolyte solution relative permittivity profiles. The horizontal black line (hidden behind the horizontal red[1] line) corresponds to the classical Poisson–Boltzmann

[1] For interpretation of color in Figs. 1–9, the reader is referred to the web version of this article.

solution: the permittivity has a constant value equal to that of water. Note that this last value is not obvious since the presence of ions generally lowers the electrolyte solution permittivity due to other reasons besides their finite size [32,33]. The red line corresponds to the modified Poisson–Boltzmann solution that only includes steric effects: ions are not allowed to come into close contact with one another or with the particle surface, but their excluded volume effect on the electrolyte solution permittivity is not taken into account. The green line corresponds to the solution that further includes the variable permittivity of the suspending medium. Close to the particle, the permittivity drops to a value that is close to the permittivity of the ions (Eq. (4) with $c_1 = c_1^{max}$). The permittivity value at even closer distances is not obvious, since ionic spheres certainly occupy part of the volume of this first exclusion layer surrounding the particle. Instead of trying to model this small distance behavior, we considered two simple limiting cases between which it certainly lies: the permittivity value for $r = a + R_1$ (lowest horizontal segment) and for $r \to \infty$ (highest horizontal segment). Finally, the orange line corresponds to the solution obtained including all the considered effects (as the green line but additionally Born and dielectrophoretic forces). Since in the considered example the presence of these forces lowers the thickness of the saturation layer but does not prevent its formation, the two values of the permittivity assigned to the exclusion layer surrounding the particle remain unaltered.

Fig. 3 shows the dimensionless electric potential profiles for the different model approximations. The black line corresponds to the classical Poisson–Boltzmann solution. The corresponding surface potential value is roughly 6 (150 mV), showing that the considered particle surface charge is not unreasonably high. The red line corresponds to the modified Poisson–Boltzmann solution incorporating just the steric effects. The potential strongly increases due to the increased thickness of the double layer that arises because of two causes: (a) the presence of a first ion exclusion layer surrounding the particle and (b) the lowering of the maximum charge density and the corresponding increase in the double layer thickness required to neutralize the fixed surface charge. Note that in the exclusion layer the charge density vanishes, so that the potential reduces to a solution of the Laplace equation. Because of this, the potential profiles in this region appear to be linear. The green line corresponds to the solution that additionally includes the effect of a variable permittivity. Close to the particle, the electric potential further increases due to the decrease in the local permittivity. The two limiting cases considered for the permittivity value in the exclusion layer are clearly visible: low permittivity value close to the ion permittivity for the upper line and high permittivity value close to the water permittivity for the lower line. On the contrary, far from the particle, the potential slightly decreases as compared to the red line. This happens because the permittivity tends to a common value in these two cases while the counterion concentration is lower for the green than for the red lines, Fig. 1, because more counterions are present in the saturation zone. Finally, the orange line corresponds to the solution obtained including all the considered effects. The electric potential slightly increases due to the action of the Born and the dielectrophoretic forces that lower the thickness of the saturation zone increasing the total double layer thickness.

Fig. 4 represents the profiles of the different forces acting on the counterions. The black lines correspond to the classical Poisson–Boltzmann solution: the solid squares represent the attractive electric force, while the empty diamonds the repulsive thermal force. These two forces exactly compensate each other at all distances. The red lines correspond to the modified Poisson–Boltzmann solution that only includes steric effects. Again, solid squares represent the attractive electric force and empty diamonds the repulsive thermal force, while solid circles represent the repulsive

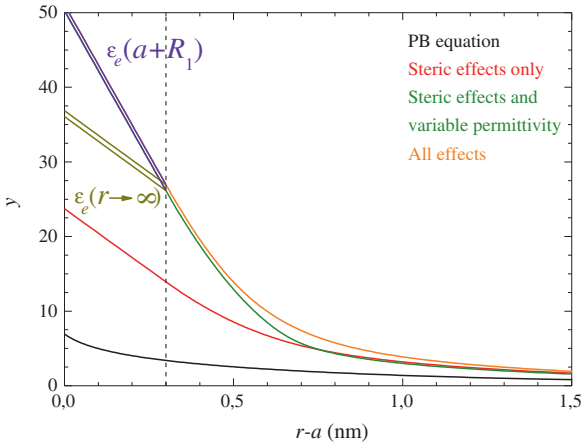

Fig. 3. Dimensionless electric potential profiles around the suspended particle for the indicated model approximations. Used parameter values given in Table 1.

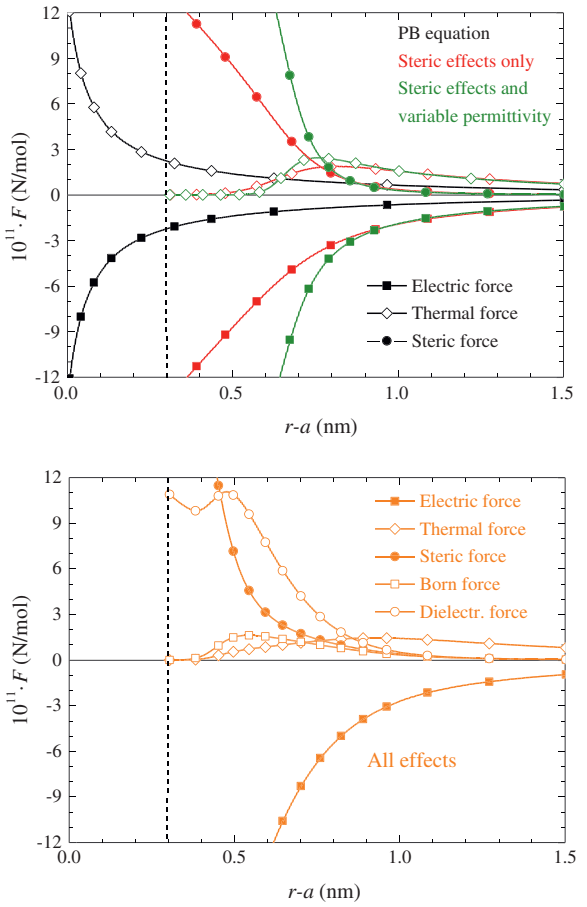

Fig. 4. Profiles of the indicated forces acting on the counterions considering the Poisson–Boltzmann solution (black lines); Poisson–Boltzmann and steric effects (red lines); Poisson–Boltzmann, steric effects, and variable permittivity (green lines); and all the considered effects (orange lines). Used parameter values given in Table 1.

steric force. Note that the thermal force (red empty diamonds) dramatically changes as compared to the classical solution (black empty diamonds) because in the saturation layer the counterion concentration becomes constant so that the thermal force vanishes. Inside this layer, the steric force (red solid circles) becomes the dominant repulsive force that compensates the attractive

electric force (red solid squares). The green lines correspond to the solution that includes both steric effects and a variable permittivity. The corresponding forces are similar to the preceding case (red lines) except for two features: (a) the electric (green solid squares) and the steric (green solid circles) forces are stronger, the first because of the electric potential increase, Fig. 3, and the second because of the increased saturation layer thickness, Fig. 1, and (b) the thermal force is stronger than in the preceding case because of the steeper concentration change outside the saturation layer, Fig. 1 (however, the green line with empty diamonds extends less toward the particle surface than the red line with empty diamonds because of the thicker saturation layer).

The lower part of Fig. 4 represents the profiles of all the forces acting on the counterions corresponding to the full solution that includes the Born and the dielectrophoretic effects. Lines with solid squares, empty diamonds, and solid circles that represent the attractive electric, the repulsive, and the repulsive steric forces are qualitatively similar to the corresponding red and green lines in the upper part of Fig. 4. The main difference is in the line representing the thermal force (empty diamonds) that is much lowered and extends further toward the particle due to the action of the repulsive Born and dielectrophoretic forces that diminish the thickness of the saturation layer, Fig. 1. The orange line with empty squares shows that the Born force is only relevant over a rather narrow distance range where the permittivity strongly changes, Fig. 2. Its magnitude strongly increases with decreasing ion size, Eq. (13), so that its relatively minor role in the considered example could become much more relevant to smaller ions. The orange line with empty circles shows that the dielectrophoretic force can be very important just outside the saturation layer, dominating all the repulsive forces. Contrary to the Born force, its magnitude increases with the ion size, Eq. (15), so that it could become negligible for smaller ions. The peculiar shape of its profile can be understood starting with the expression of the dielectrophoretic force, Eq. (15), written as:

$$F_i^D = 4\pi\varepsilon_e R_i^3 \frac{\varepsilon_i - \varepsilon_e}{\varepsilon_i + 2\varepsilon_e}\left(-\frac{d\Psi}{dr}\right)(-\nabla^2\Psi)$$

Combining this expression with Eq. (5) gives

$$F_i^D \approx -4\pi R_i^3 \frac{\varepsilon_i - \varepsilon_e}{\varepsilon_i + 2\varepsilon_e}\frac{d\Psi}{dr}\left(z_1 e c_1 + \frac{d\Psi}{dr}\frac{d\varepsilon_e}{dr}\right) \tag{34}$$

where the influence of co-ions was neglected. In the considered example, the fixed particle surface charge is positive so that both $d\Psi/dr$ and $z_1 e c_1$ are negative while $d\varepsilon_e/dr$ is positive. Inside the saturation layer, both the counterion concentration and the electrolyte solution permittivity are constant, Figs. 1 and 2, so that the force diminishes because the derivative of the electric potential diminishes (in modulus), Fig. 3. This leads to the initial decrement of the orange line with empty circles in Fig. 4. At greater distances, close to the outer boundary of the saturation layer, the counterion concentration starts to decrease, Fig. 1, while the permittivity starts to increase, Fig. 2. This competing behavior of the two addends inside the parenthesis in Eq. (34) produces an increase in this term over a limited distance range which leads to a maximum of the dielectrophoretic force.

Fig. 5 shows the influence on the obtained results of the permittivity value assigned to the dielectric spheres representing the ions. This value has obviously no bearing on the Poisson–Boltzmann (black lines) and Poisson–Boltzmann with steric effects (red lines) solutions. When the variable permittivity effect is taken into account, a high $\varepsilon_i = 40\varepsilon_0$ value leads to small changes of the electrolyte solution permittivity so that the green and orange lines remain close to the red line in Fig. 5b. However, lowering the ion permittivity value to $\varepsilon_i = 10\varepsilon_0$ strongly lowers the electrolyte solution permittivity, which increases the radial electric field of the particle

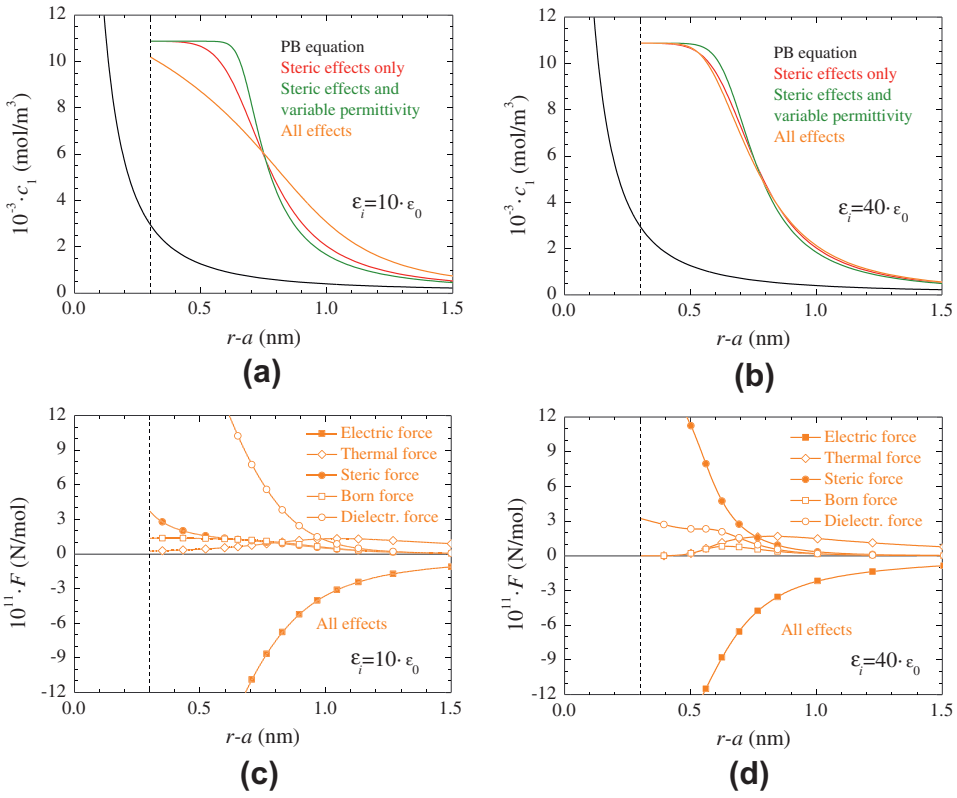

Fig. 5. Dependence of the counterion concentration and the different force profiles on the permittivity value assigned to the ionic sphere. Used parameter values given in Table 1 except for $\varepsilon_i = 10\varepsilon_0$ (a and c) and $\varepsilon_i = 40\varepsilon_0$ (b and d).

that attracts more counterions to the saturation layer. When only the variable permittivity effect is considered, this increases the saturation layer thickness, green line in Fig 5a. On the contrary, when all the effects are taken into account, orange line in Fig. 5a, the Born and the dielectrophoretic repulsive forces are stronger than the increase in the electric force causing a decrease in the saturation layer thickness. Actually, in the considered example, the effect of these forces becomes so strong that the saturation layer vanishes altogether: the counterion concentration no longer attains the c_1^{max} value.

Both for $\varepsilon_i = 10\varepsilon_0$ and for $\varepsilon_i = 40\varepsilon_0$, the Born force is very small (orange lines with empty squares in Fig. 5c and d) mainly due to the relatively large ion size. The main repulsive forces are the dielectrophoretic and then steric for $\varepsilon_i = 10\varepsilon_0$ (empty diamonds and solid circles in Fig. 5c). This order reverses for $\varepsilon_i = 40\varepsilon_0$ when the steric becomes the strongest repulsive force followed by the dielectrophoretic force (solid circles and empty diamonds in Fig. 5d). The reason for this change is in the absence of the saturation layer in the first case and its presence in the second one. For $\varepsilon_i = 10\varepsilon_0$, the dielectrophoretic force becomes strong because of the strong variation of the electrolyte solution permittivity, Eq. (34), while the steric force is low because the counterion concentration is far from its c_1^{max} value, Eqs. (10) and (11). The opposite situation arises for $\varepsilon_i = 40\varepsilon_0$: strong steric force in the close vicinity of the saturation layer and weak dielectrophoretic force inside this layer where the electrolyte solution permittivity has a constant value.

Fig. 6 shows the dependence of the obtained results on the ion size. For $R_i = 0.1$ nm, there is no saturation layer because of the very high c_1^{max} value corresponding to this small ion radius, Eq. (3). Note that in Fig. 6a, the maximum ion concentration value obtained considering steric effects is practically the same as according to the Poisson–Boltzmann equation. The opposite situation is observed in Fig. 6b for the large $R_i = 0.5$ nm ion radius: a thick saturation layer with a c_1^{max} value that is roughly 40 times smaller than the maximum Poisson–Boltzmann concentration.

The corresponding forces acting on the counterions have also quite different behaviors. For $R_i = 0.1$ nm, Fig. 6c, the thermal force is the dominant repulsive force (just as in the classical description) followed by the Born force that increases because of the small ion size, Eq. (13). On the contrary, the dielectrophoretic and the steric forces are almost negligible, the first because of the small ion size, Eq. (15), and the second because of the low ion concentration as compared to c_1^{max}, Eqs. (10) and (11). The opposite situation can be seen in Fig. 6d corresponding to $R_i = 0.5$ nm: the dominant repulsive force is steric followed by the dielectrophoretic force that increases because of the large ion radius. On the contrary, the thermal and the Born forces are almost negligible, mainly because of the constant ion concentration and electrolyte solution permittivity across the saturation layer.

Fig. 7 shows the surface potential as a function of the surface charge. The black line represents the Poisson–Boltzmann solution, the red line represents the solution obtained taking into account steric effects, the green lines incorporate furthermore the effects due to a variable permittivity of the electrolyte solution, while the orange lines additionally consider the Born and the dielectrophoretic forces. In these last two cases, two solutions are presented corresponding to the value assigned to the permittivity in the ion exclusion layer: equal to the permittivity value far from the particle, solid circles, or to the value calculated at $r = a + R_1$, open circles. As can be seen, all the considered effects increase the surface potential as compared to the Poisson–Boltzmann solution. Moreover, the consideration that ions behave as dielectric spheres further increases the surface potential as compared to the assumption that steric effects only limit the ability of ions to come close to one another and to the particle surface. For low surface charges, the dominant cause for the increase in the surface

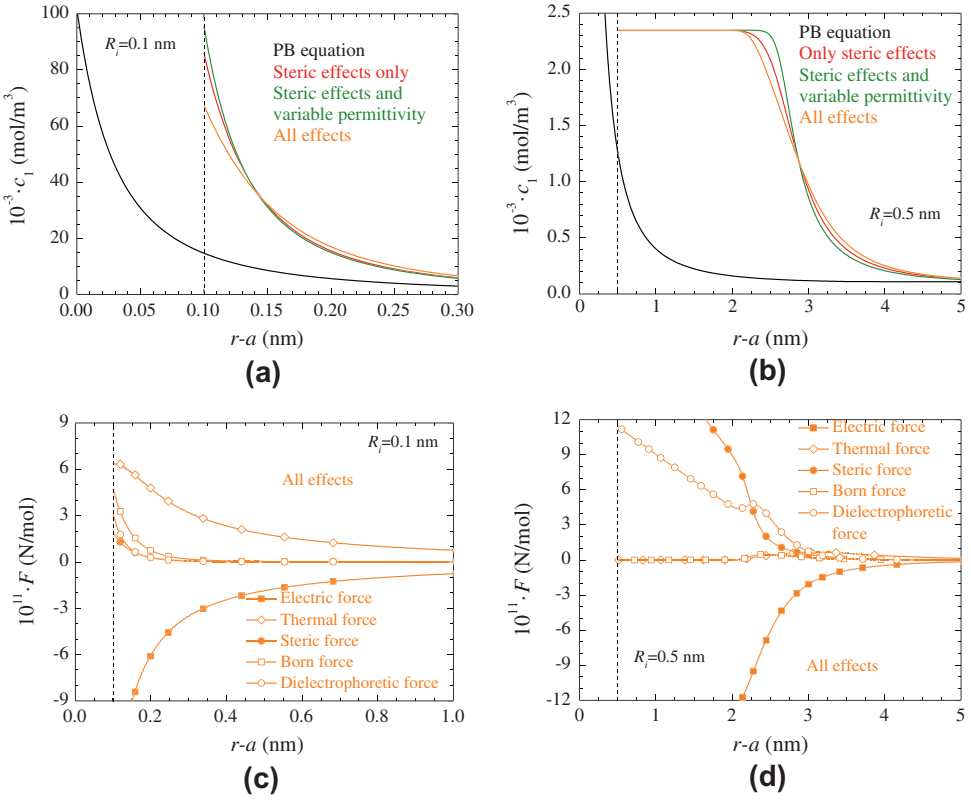

Fig. 6. Dependence of the counterion concentration and the different force profiles on the ionic radius. Used parameter values given in Table 1 except for $R_i = 0.1$ nm ((a) and (c)) and $R_i = 0.5$ nm ((b) and (d)).

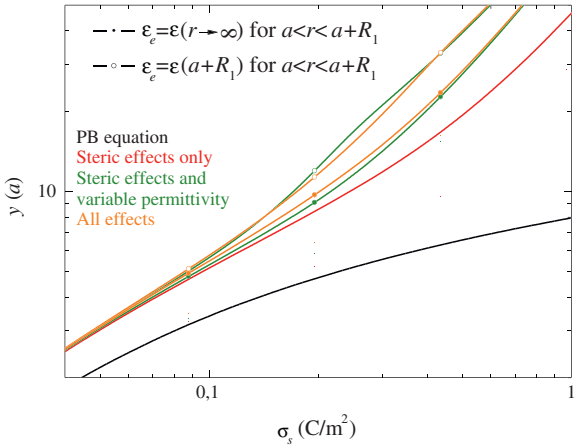

Fig. 7. Dimensionless surface potential as a function of the surface charge for the indicated model approximations. Remaining parameters given in Table 1.

potential is the finite minimum approach distance of ions to the particle surface. For high surface charges, this increase is a complex function of all the considered effects: the maximum allowed ion concentration that causes the formation of the saturation layer, the local variation of the electrolyte solution permittivity and the corresponding increase in the attractive electric force acting on the counterions, and the appearance of the repulsive Born and dielectrophoretic forces. Finally, the effective value of the electrolyte solution permittivity inside the ion exclusion layer has also a strong bearing on the surface permittivity at high surface charges (this difference disappears at low surface charges because the electrolyte solution permittivity at $r = a + R_1$, Fig. 2, tends then to the corresponding permittivity far from the particle for low ion concentrations).

Fig. 8 shows the surface potential as a function of the surface charge and its dependence on the ion permittivity value. In order to better appreciate the magnitude of the observed effects, linear rather than logarithmic scales are used for both axes. Note that the surface charges considered are quite realistic since they lead to Poisson–Boltzmann surface potential values in the 0–200 mV range. As expected, the surface potential strongly increases when the ion permittivity value decreases since all the discussed effects are related to the electrolyte solution permittivity variation.

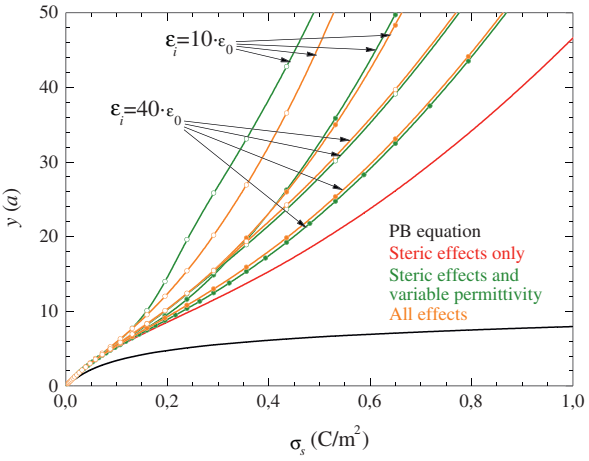

Fig. 8. Dimensionless surface potential as a function of the surface charge and its dependence on the permittivity value assigned to the ionic sphere. Solution permittivity values used for $a < r < a + R_1$: $\varepsilon_e = \varepsilon_e(r \to \infty)$, solid circles, $\varepsilon_e = \varepsilon_e(a + R_1)$, empty circles. Remaining parameters given in Table 1.

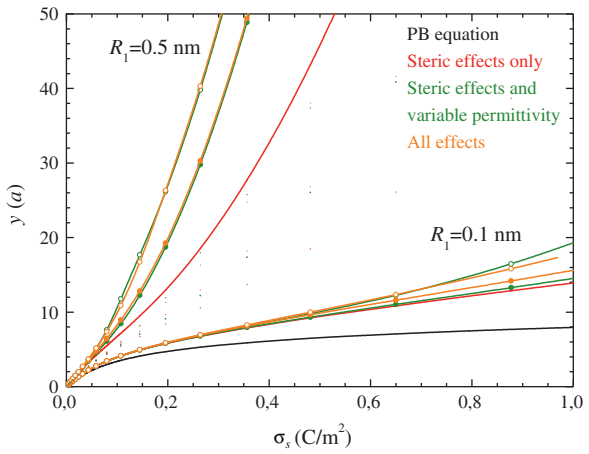

Fig. 9. Dimensionless surface potential as a function of the surface charge and its dependence on the ionic radius. Solution permittivity values used for $a < r < a + R_1$: $\varepsilon_e = \varepsilon_e(r \to \infty)$, solid circles, $\varepsilon_e = \varepsilon_e(a + R_1)$, empty circles. Remaining parameters given in Table 1.

Because of this, the surface potential values converge to the results obtained considering only steric effects when the ion permittivity approaches the water permittivity value. It should be noted, however, that even for the relatively high $\varepsilon_i = 40\varepsilon_0$ value, the contribution due to all the effects related to the electrolyte solution permittivity variation is far from negligible.

Fig. 9 shows the surface potential as a function of the surface charge and its dependence on the ion size. As can be seen, the surface potential roughly doubles even for the small $R_1 = 0.1$ nm ion size, while for $R_1 = 0.5$ nm, it increases by nearly an order of magnitude. This increment strongly depends on the presence of the steric effects, on the local variation of the electrolyte solution permittivity, and on the permittivity value of the ion exclusion layer. However, it is almost independent of the inclusion of the Born and the dielectrophoretic forces: the green and orange lines nearly coincide just as in Fig. 3.

4. Conclusion

We present a detailed account of the equilibrium properties for a charged spherical colloidal particle immersed in an aqueous electrolyte solution. We use an extension of the Standard Electrokinetic Model that removes the classical assumption that ions behave as mathematical points. The finite ion size has been taken into account in many earlier works by restricting their ability to approach one another [12–18] and the surface of the particle [21–23]. We further consider that a finite size implies that ions should behave as dielectric spheres, which leads to the following consequences:

(a) The excluded volume occupied by the ions modifies the local value of the electrolyte solution permittivity.
(b) The resulting permittivity gradients lead to the appearance of a Born force that tends to move ions toward regions of higher permittivity.
(c) Ions get polarized by the local electric field and are acted upon by a dielectrophoretic force that is proportional to the field gradient.

All these features are incorporated into the model that is numerically solved. The obtained results make it possible to analyze the individual forces acting over the ions. The attractive electric force is always important and increases with decreasing electrolyte solution permittivity. The repulsive thermal force, which in the

classical formulation exactly opposes the electric force, is usually strongly diminished and actually vanishes wherever the ion concentration attains its maximum value. The steric repulsive force becomes dominant precisely in these regions of high ion concentration. The repulsive Born force is usually small but becomes important for small ions. And the dielectrophoretic repulsive force can surpass all the other repulsive forces for large ions.

The considered effects have an important bearing on the surface potential value: at any given surface charge, this potential always increases with respect to the classical Poisson–Boltzmann solution when steric effects are taken into account. We show that the modeling of ions as dielectric spheres leads to an additional increase in comparable magnitude. This suggests that a solution of the presented model under nonequilibrium conditions could have important consequences in the interpretation of dielectric and electrokinetic data in colloidal suspensions.

Acknowledgments

The authors wish to acknowledge financial support for this work provided by MICINN (Project FIS2010-19493) and Junta de Andalucía (Project PE-2008 FQM-3993) of Spain, co-financed with FEDER funds by EU, and by CIUNT (Project 26/E419) of Argentina.

References

[1] D. Andelman, Electrostatic properties of membranes: the Poisson–Boltzmann theory, in: R. Lipowsky, E. Sackmann (Eds.), Handbook of Biological Physics, 1, Elsevier Science, Amsterdam, 1995 (Chapter 12).
[2] D.F. Evans, H. Wennerström, The Colloidal Domain, VCH Publishers, NewYork, 1994.
[3] R.J. Hunter, Zeta Potential in Colloid Science. Principles and Applications, Academic Press, London, 1981.
[4] G. Gouy, J. Phys. Theor. Appl. 9 (1910) 457.
[5] D.L. Chapman, Philos. Mag. 25 (1913) 475.
[6] P. Debye, E. Hückel, Physik Z. 24 (1923) 185.
[7] F. Booth, J. Chem. Phys. 19 (1951) 821.
[8] A.L. Loeb, P.H. Wiersema, J.Th.G. Overbeek, The Electrical Double Layer around a Spherical Colloid Particle, MIT Press, Cambridge, Mass, 1961.
[9] H. Ohshima, T.W. Healy, L.R. White, J. Colloid Interface Sci. 90 (1982) 17.
[10] J.J. López-García, A.A. Moya, J. Horno, A. Delgado, F. González-Caballero, J. Colloid Interface Sci. 183 (1996) 124.
[11] J. Lyklema, Fundamentals of Colloid and Interface Science, Solid/Liquid Interfaces, II, Academic Press, London, 1995.
[12] I. Borukhov, D. Andelman, H. Orland, Phys. Rev. Lett. 79 (1997) 435.
[13] S. Woelki, H.H. Kohler, Chem. Phys. 261 (2000) 411.
[14] K. Bohinc, V. Kralj-Iglic, A. Iglic, Electrochim. Acta 46 (2001) 3033.
[15] P.M. Biesheuvel, Eur. Phys. J. E. 16 (2005) 353.
[16] J.J. López-García, M.J. Aranda-Rascón, J. Horno, J. Colloid Interface Sci. 316 (2007) 196.
[17] P.M. Biesheuvel, M. van Soestbergen, J. Colloid Interface Sci. 316 (2007) 490.
[18] L.B. Bhuiyan, C.W. Outhwaite, J. Colloid Interface Sci. 331 (2009) 543.
[19] J.G. Ibarra-Armenta, A. Martín-Molina, M. Quesada-Pérez, Phys. Chem. Chem. Phys. 11 (2009) 309.
[20] J.J. López-García, M.J. Aranda-Rascón, J. Horno, J. Colloid Interface Sci. 323 (2008) 146.
[21] M.J. Aranda-Rascón, C. Grosse, J.J. López-García, J. Horno, J. Colloid Interface Sci. 335 (2009) 250.
[22] M.J. Aranda-Rascón, C. Grosse, J.J. López-García, J. Horno, J. Colloid Interface Sci. 336 (2009) 857.
[23] J.J. López-García, M.J. Aranda-Rascón, C. Grosse, J. Horno, J. Phys. Chem. B 114 (2010) 7548.
[24] E.R. Nightingale, J. Phys. Chem. 63 (1959) 1381.
[25] M.Z. Bazant, M.S. Kilic, B.D. Storey, A. Ajdari, Adv. Colloid Interface Sci. 152 (2009) 48.
[26] J.J. López-García, C. Grosse, J. Horno, Langmuir 27 (2011) 13970.
[27] J.C. Maxwell, A Treatise on Electricity and Magnetism, 1, Clarendon, Oxford, 1892.
[28] M.M. Hatlo, R. van Roij, L. Lue, Eur. Phys. Lett. 97 (2012) 28010.
[29] M. Born, Z. Phys. 1 (1920) 45.
[30] J.J. Bikerman, Philos. Mag. 33 (1942) 384.
[31] S. Gavryushov, J. Phys. Chem. B 112 (2008) 8955.
[32] J. Hubbard, L. Onsager, J. Chem. Phys. 67 (1977) 4850.
[33] J. Hubbard, L. Onsager, J. Chem. Phys. 68 (1978) 1649.